SolarPACES 2022, 28th International Conference on Concentrating Solar Power and Chemical Energy Systems
Power Cycles
https://doi.org/10.52825/solarpaces.v1i.762

Published: 15 Mar. 2024

Direct Optimization for Cycle Working Fluids using a Thermodynamic Generalized Fluid Approach

Justin Begay[1], and Daniel T. Banuti[2][https://orcid.org/0000-0002-5469-5704]

[1] University of New Mexico, NM, USA

[2] Karlsruhe Institute of Technology (KIT), Institute for Thermal Energy Technology and Safety (ITES), Germany

Abstract. Fluid blends as working fluids in solar thermal power cycles have been shown to promise an even higher efficiency than pure fluids. Rather than exploring specific blends, we propose an approach in which we directly optimize for a working fluid characterized in terms of the fluid critical point following the fundamental corresponding states principle. This direct approach allows to identify the optimal fluid one would require for given cycle boundary conditions. The approach can be applied to any given cycle; the suitable fluid selection is then performed in a second step after the desired optimal properties are identified.

Keywords: Thermodynamics, Power Cycles, ORC, CO2,

1. Introduction

Using different working fluids in cycle optimization provides an additional parameter that can be used to improve cycle efficiency. In the past, different fluids have been used, such as steam [1], carbon dioxide [2], or organic compounds [3]. Particularly for thermal solar power applications based on molten salt energy storage, working fluid choice is an active topic of research [3,4]. More recently, mixtures as working fluids are being explored [6-8] for solar power applications. Valencia-Chapi [6] explored a wider range of mixtures, including hydrocarbons and noble gases. Crespi et al. [5] investigated blends of CO_2 with C_6F_6 and $TiCl_4$, where the additive takes up mole fractions of 10, 15, or 20%. Crespi et al.'s study concluded that super CO_2 (sCO_2) mixtures performed better than a conventional sCO_2 power cycle for the same boundary conditions. Their study had a thermal efficiency increase of 4-5%. Moreover, Crespi's team confirmed thermal efficiencies greater than 50%. The cycle they investigated had minimum temperatures ranging from 50◦C to 55◦C. Ultimately, the impact of the mixture is to change the critical point of the working fluid, which affects the efficiency of the cycle. While these studies shed a crucial light on the direction of future power cycle technology, the question arises, 'how can we optimally decide which fluid mixture will provide the most thermally efficient power cycle?' So far, optimization of these blended working fluids is exploratory, in which different fixed compositions are compared [5], or binary mixtures with variable compositions are evaluated [6]. Both approaches rely on a restriction of the optimization space to preselected fluids.

In the present paper, we propose an inverse approach instead: rather than choosing specific components of a blended working fluid, an optimal critical point of a virtual working fluid can directly be optimized for, with a choice of blends that fulfill that property as a second, independent step. More specifically, this method has the ability to take a documented cycle that has well-defined cycle constraints, i.e. a fixed higher and lower operating pressure, and a

fixed temperature into the turbine (TIT), and determine a virtual working fluid with a critical temperature and pressure that produces the optimal thermal efficiency.

2. Method

Thermodynamically, our approach is based on the corresponding states principle [1], in which fluid properties are similar between different fluids when normalized to the respective reduced values, e.g. the reduced pressure p_r is pressure p normalized with the critical pressure, p_{cr}. i.e., we are not restricted to using fluid properties of certain (existing) species.

Studying molecular behavior from a molecular interactions point of view reveals that molecules can be grouped into classes. Within each of these classes, there are similarities between molecular interactions. Similarities among the dipole-dipole interactions, dispersion forces, and hydrogen bonding exist between these molecules. Furthermore, a number of different molecules that belong to the same class may be represented by a common volumetric equation of state [8]. The van der Waal's equation of state extends the ideal gas law to account for the intermolecular forces between the molecules and the finite size of the molecules. The ideal gas law is represented by, $p\,\frac{V}{n} = RT$, where p is the pressure, V is the volume, n is the amount of moles, R is the gas constant, and T is the temperature. To account for finite volume that is associated with the molecules, $\frac{V}{n}$ is replaced with $V_m - b$. V_m represents the molar volume and b represents a constant that was proposed by J.D. van der Waals [8]. To account for the intermolecular forces between the molecules, the term $\frac{a}{V_m^2}$ was added to the pressure. Similar to b, the a term is a constant that was proposed by van der Waals. These constants depend on the type of molecule that is being considered. The van der Waals equation of state is now [8]:

$$(p + \tfrac{a}{V_m^2})(V_m - b) = RT \tag{1}$$

The van der Waals coefficient a can be expressed as, $a = 3\,p_c\,V_c^2$. The b coefficient can be expressed as, $b = \frac{V_c}{3}$. The reduced parameters are expressed as: $T_r = \frac{T}{T_c}$, $p_r = \frac{p}{p_c}$, and $V_r = \frac{V}{V_c}$, and substituting these reduced parameters along with the van de Waals coefficients into equation (1) yields:

$$(p_r + \tfrac{3}{V_r^2})\,(3V_r - 1) = 8\,T_r \tag{2}$$

The van der Waals equation of state is not universally applicable. In reality, not all fluids have a similar shape and intermolecular forces. Rather, the sphericity and intermolecular interaction of fluids can differ significantly. Hence, Pitzer et al. [9] proposed an additional independent variable to the corresponding states principle, the acentric factor. The acentric factor is denoted with ω. Pitzer et al. claimed that fluids that have similar acentric factors may adhere to the corresponding states principle and be represented by the same equation of state. As an example, the compressibility, Z, of two fluids with similar acentric factors will be plotted as a demonstration of the corresponding states principle. Nitrogen has an acentric factor of 0.04 and Oxygen has an acentric factor of 0.021.

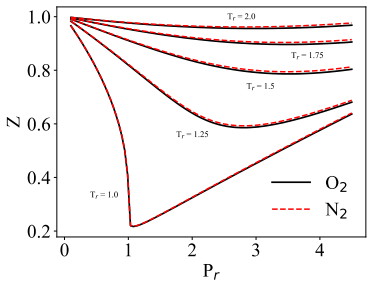

Figure 1. The compressibility factor, Z, of Oxygen and Nitrogen are plotted as a function of the reduced pressure, p_r.

The acentric factors for O_2 and N_2 are small and close in value; therefore, they can be arranged together into the same class. The compressibility factor for both fluids closely resemble each other. The compressibility factor is the ratio of molar volume of a fluid to the molar volume of an ideal gas. It is important because it describes the divergence of the real gas from ideal gas behavior. Figure 1 illustrates how, at a reduced state, both of these fluids deviate from ideal gas behavior in a similar manner which demonstrates the corresponding states principle. The concept of the corresponding states principle is a key connection within the project idea because it argues that fluids can behave similarly to a certain extent.

Now, the evaluation is carried out by extending the open source CoolProp fluid property library [7] with our generalized fluids method using variable critical points. The goal is to develop a method that characterizes a virtual fluid by an equation of state. In doing so, the key features that CoolProp uses to characterize a fluid will be determined and a method that makes thermal efficiency become a function of T_c and p_c will arise. The Soave-Redlich-Kwong equation of state was chosen to work with and it is defined as [10],

$$p = \frac{RT}{V_m - b} - \frac{a\,\alpha}{V_m\,(V_m + b)} \tag{3}$$

In this equation of state, $a = \frac{0.42747\,R^2\,T_c^2}{p_c}$, $b = \frac{0.08664\,R\,T_c}{p_c}$, $\alpha = (1 + (0.48508 + 1.55171\omega - 0.15613\,\omega^2)(1 - T_r^{0.5}))^2$. The Soave-Redlich-Kwong equation of state is a useful tool that relates the pressure, temperature, and volume of a fluid. Although this is helpful, the objective is to generate values of specific entropy and enthalpy that will be used to calculate the thermal efficiency of the cycle. The relationship between the equation of state and specific entropy and enthalpy values lies within Helmholtz energy. CoolProp uses the equation of state that is explicit in the reduced Helmholtz energy. The other thermodynamic properties are calculated through derivatives of the Helmholtz energy [11]. Thus, it is important to consider the Helmholtz energy term and its components. When discussing the Helmholtz energy term, the reduced temperature will be denoted as τ, the Helmholtz energy as α, the reduced density as δ, the enthalpy as h, the entropy as s, the isobaric heat capacity as c_p, the internal energy as u, and the molecular partition function as q.

$$\frac{h}{RT} = \tau\left(\left(\frac{\partial\alpha^0}{\partial\tau}\right)_\delta + \left(\frac{\partial\alpha^r}{\partial\tau}\right)_\delta\right) + \delta\left(\frac{\partial\alpha^r}{\partial\delta}\right)_\tau + 1 \tag{4}$$

$$\frac{s}{R} = \tau\left(\left(\frac{\partial\alpha^0}{\partial\tau}\right)_\delta + \left(\frac{\partial\alpha^r}{\partial\tau}\right)_\delta\right) - \alpha^0 - \alpha^r \tag{5}$$

Equations (4) and (5) illustrate the relationship between the Helmholtz energy term and the specific enthalpy and entropy. A major objective of the project is to fully characterize a virtual fluid in a way that adjusting T_c and p_c will cause a change in the thermal efficiency. In order to meet the goal, the ideal gas reference term, α^0, needs to be determined. The ideal gas reference term is defined as:

$$\alpha^0 = h^0 - RT - Ts^0 \quad (6)$$

In equation (6), $h^0 = h_0^0 + \int_{T_0}^{T} c_p^0 dT$ and $s^0 = s_0^0 + \int_{T_0}^{T} \frac{c_p^0}{T} dT - R \ln \frac{\rho T}{\rho_0 T_0}$. Substituting these definitions into equation (6) and using the reduced variables results in the Helmholtz energy being expressed as,

$$\alpha^0 = \frac{h_0^0 \tau}{RT_c} - \frac{s_0^0}{R} - 1 + \ln \frac{\delta \tau_0}{\delta_0 \tau} - \frac{\tau}{R} \int_{\tau_0}^{\tau} \frac{c_p^0}{\tau^2} d\tau + \frac{1}{R} \int_{\tau_0}^{\tau} \frac{c_p^0}{\tau} d\tau \quad (7)$$

The heat capacity term, c_p^0 , is defined as:

$$\frac{c_p^0}{R} = \frac{5}{2} + \frac{d}{dT}\left(T^2 \frac{d \ln q}{dT}\right) \quad (8)$$

The following equation has been determined to calculate values within 0.01% when compared to equation (8) [11].

$$\frac{c_p^0}{R} = a_0 + a_1 T + a_2 T^2 + a_3 T^3 + a_4 \frac{u^2 exp(u)}{(exp(u)-1)^2} \quad (9)$$

Substituting equation (9) into equation (7), the following simplified equation emerges [11]:

$$\alpha^0 = \ln \delta + a_1 \ln \tau + a_2 + a_3 \tau + a_4 \tau^{-1} + a_5 \tau^{-2} + a_6 \tau^{-3} + a_7 \ln(1 - exp(-a_8 \tau)) \quad (10)$$

For the purposes of this project, the heat capacity will be considered constant and not a function of *T*. Thus, equation (8) becomes $\frac{c_p^0}{R} = \frac{5}{2}$. Also, a constant heat capacity incorporated into equation (7) yields, $\alpha^0 = \frac{h_0^0 \tau}{RT_c} - \frac{s_0^0}{R} - 1 + \ln \frac{\delta \tau_0}{\delta_0 \tau} - \frac{\tau c_p^0}{R} \int \frac{1}{\tau^2} d\tau + \frac{c_p^0}{R} \int \frac{1}{\tau} d\tau$. Taking the integral of this equation results in,

$$\alpha^0 = \frac{h_0^0 \tau}{RT_c} - \frac{s_0^0}{R} - 1 + \ln \frac{\delta \tau_0}{\delta_0 \tau} - \frac{c_p^0}{R} + \frac{c_p^0}{R} \ln \tau \quad (11)$$

Simplifying equation (11) results in,

$$\alpha^0 = \ln \delta + a_1 \ln \tau + a_2 + a_3 \tau \quad (12)$$

Where a_1 is $\frac{c_p^0}{R}$ which is 2.5, and a_2 and a_3 are determined by experimental data [11]. This section reduces the relatively long and specific α^0 function to three terms, making it simpler and more general. Now, the virtual fluid can be fully characterized in CoolProp, and the entropies and enthalpies are a function of T_c and p_c.

3. Results

To verify that the simplified and generalized $\boldsymbol{\alpha^0}$ function returns accurate entropies and enthalpies, a virtual fluid will be created and compared to NIST [12] reference data. The virtual fluid will be constructed based on characteristics of a low acentric fluid, nitrogen. For verification purposes, the virtual fluid will be defined with a T_c of 126.2 and a p_c of 3.39 MPa, which aligns with the critical parameters of nitrogen. After the virtual fluid has been constructed with the aforementioned critical parameters, the values of specific entropy and enthalpy of that fluid will be compared to reference data.

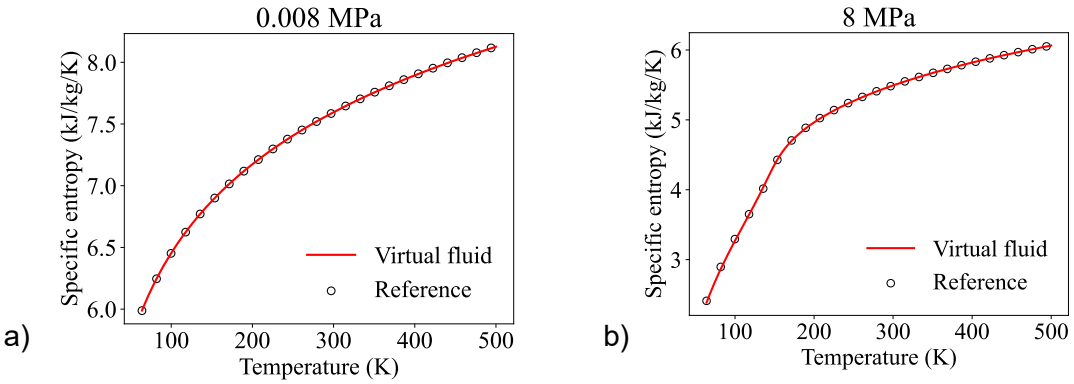

a) b)

Figure 2. Validation of the method by comparing the virtual fluid (red solid line) to reference data (symbols) of nitrogen for subcritical (a) and supercritical (b) pressures.

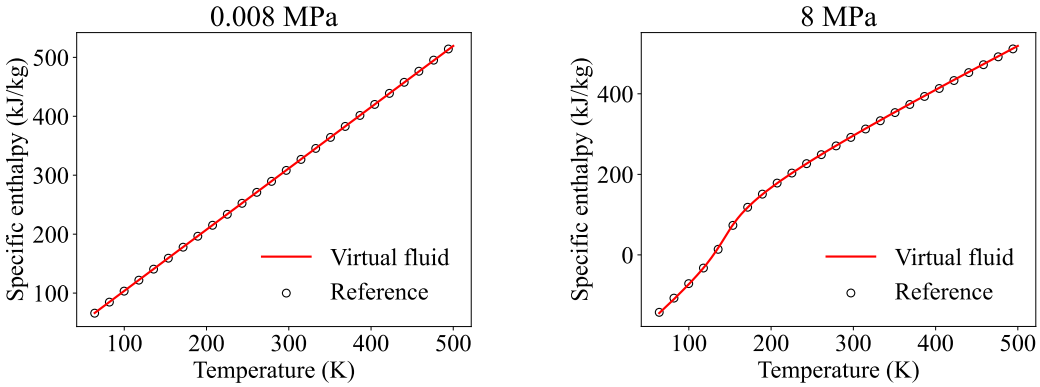

a) b)

Figure 3. Validation of the method by comparing the virtual fluid (red solid line) to reference data (symbols) of nitrogen for subcritical (a) and supercritical (b) pressures.

Figures 2 and 3 validate the concept by demonstrating that the generalized fluid properties accurately match real fluid reference data. To demonstrate that adjusting the critical parameters causes a shift in the thermal efficiency of the cycle, the specific entropy and enthalpy of a virtual fluid with different T_c and p_c values will be plotted against each other.

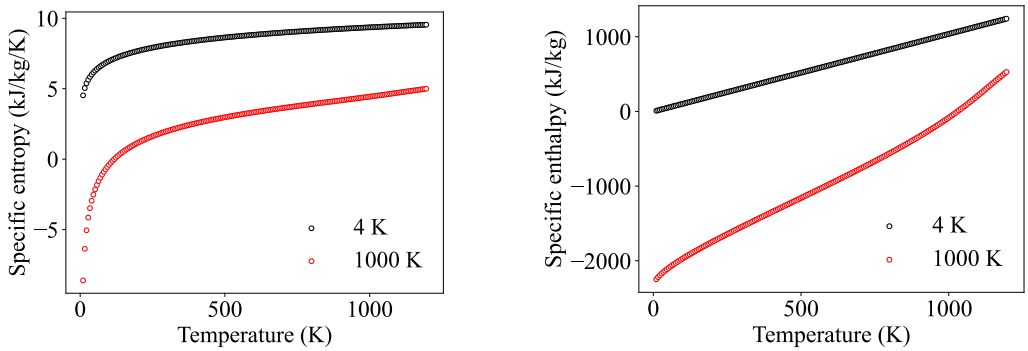

a) b)

Figure 4. Proof of concept showing specific entropy and enthalpy changes when comparing the virtual fluid with a T_c of 1000 K (red symbols) to a virtual fluid with a T_c of 4 K (black symbols).

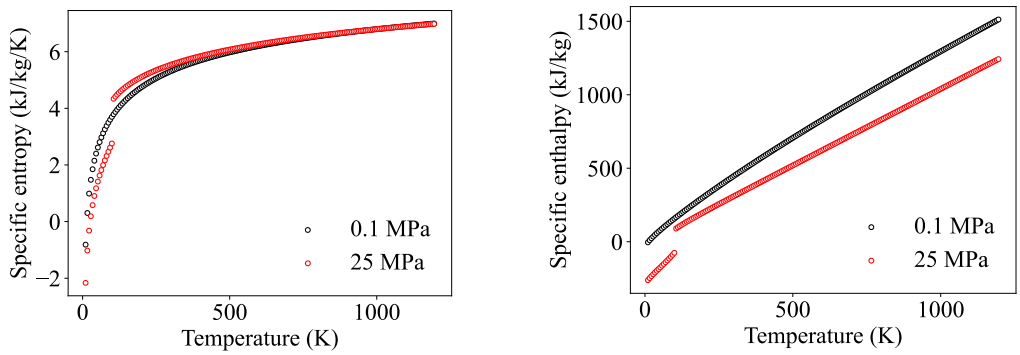

a) b)

Figure 5. Proof of concept showing specific entropy and enthalpy changes when comparing the virtual fluid with a p_c of 25 MPa (red symbols) to a virtual fluid with a p_c of 0.1 MPa (black symbols).

Figures 4 and 5 illustrate the variance of the specific entropy and enthalpy when T_c and p_c are modified. The thermal efficiency of a Rankine cycle is determined by dividing the net work of the system by the heat added into the system. The net work can be determined by finding the enthalpy differences across the turbine and pump and subtracting these numbers, $(\boldsymbol{h_{bef\ exp}} - \boldsymbol{h_{aft\ exp}}) - (\boldsymbol{h_{aft\ comp}} - \boldsymbol{h_{bef\ comp}})$. The amount of heat added into the system can be determined by finding the enthalpy difference across the heat addition device, $\boldsymbol{h_{aft\ heat\ add}} - \boldsymbol{h_{bef\ heat\ add}}$. Finally, the thermal efficiency of the cycle is determined by taking the ratio of these two quantities. Therefore, demonstrating a difference in specific entropy and enthalpy values verifies that there will be a difference in cycle thermal efficiencies when adjusting T_c and p_c. Now, the method will be applied on an actual Rankine cycle with pressure and temperature boundary conditions. The Rankine cycle of interest consists of a higher pressure limit of 8 MPa, and a lower pressure limit of 0.008 MPa. The temperature into the turbine is fixed at 568.16 K, and after heat has been rejected causing the working fluid to get condensed, the fluid will be at a saturated liquid state [13].

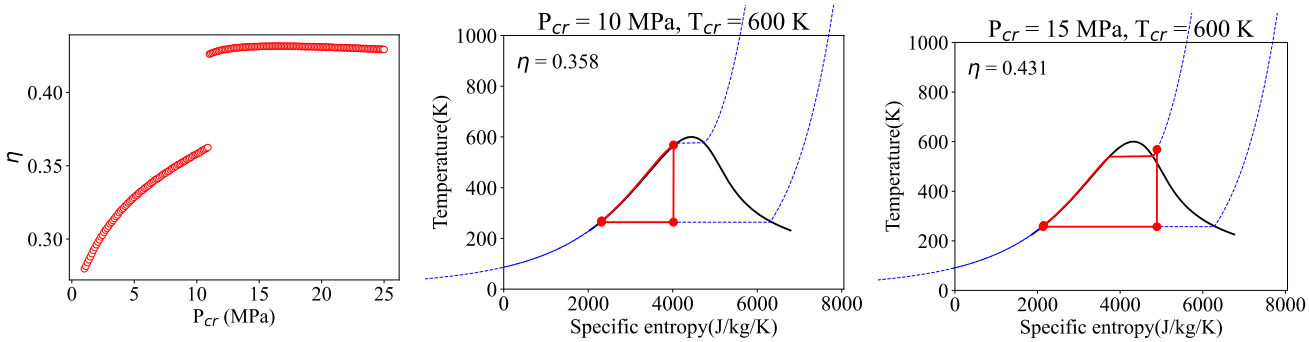

a) b) c)

Fig. 6: Application of the method to the optimization of a Rankine cycle with a higher working pressure of 8 MPa, a lower working pressure of 0.008 MPa, and a TIT of 568.16 K. For this demonstration, the critical temperature of the generalized working fluid is fixed at 600 K.

Figure 6 illustrates the application of the method towards the optimization of a working fluid for a Rankine cycle. The distribution of the thermal efficiency, Fig. 6a, provides two distinct features: A distinct jump of the efficiency from 0.36 to 0.41 is visible at p_{cr} ~ 11 MPa, which can be associated with an expansion at supercritical entropies, as seen between Figs. 6b and 6c. A maximum is visible for a working fluid critical pressure of ~ 15 MPa. The method can be used to simultaneously optimize for the critical temperature, critical pressure, and the acentric factor.

Another system configuration that is considered is one where there are upper and lower limits for both the operating temperatures and pressures. The upper operating temperature for this configuration is the TIT and the lower operating temperature is the temperature into the pump. In this system configuration, the cycle is able to interchange between a Rankine cycle and a Brayton cycle, which depends on the selection of T_c and p_c. The system that will be used is a hybrid parabolic solar dish power plant [14], which has solar applications. The solar dish consists of a TIT of 823.15 K, and a temperature of 313.15 K prior to entering the pump. The upper limit of the operating pressure is 1.2 MPa, and the lower limit of the operating pressure is 0.05 MPa.

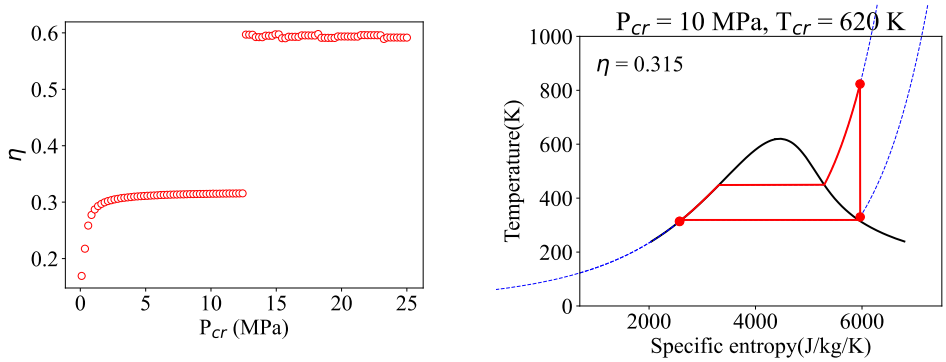

a) b)

Figure 7. Application of the method to the optimization of a hybrid parabolic solar dish power plant. The thermal efficiency plotted as a function of p_c (a). Ts diagram illustrating the Rankine cycle when the virtual working fluid has p_c of 10 MPa (b). For this demonstration, the critical temperature of the generalized working fluid is fixed at 620 K.

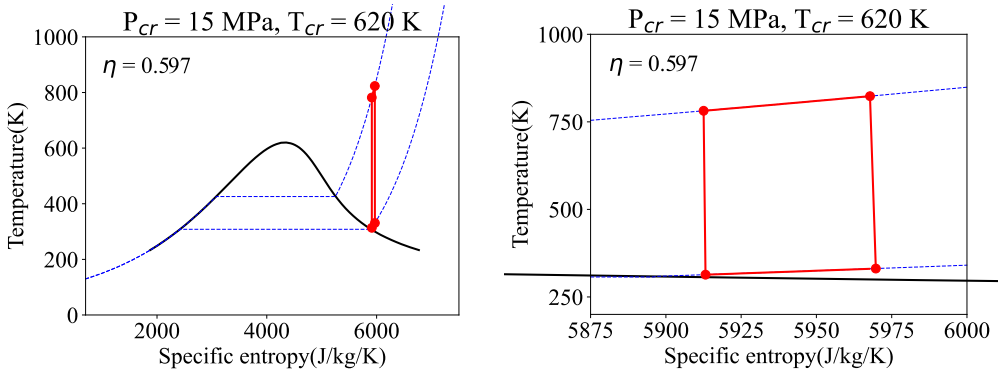

a) b)

Figure 8. Application of the method to the optimization of a hybrid parabolic solar dish power plant. Ts diagram illustrating the Brayton cycle when the virtual working fluid has a p_c of 15 MPa (a). Zoomed in Ts diagram demonstrating the Brayton cycle when the virtual working fluid has a p_c of 15 MPa (b). For this demonstration, the critical temperature of the generalized working fluid is fixed at 620 K.

Figures 7 and 8 illustrate the application of the method towards the optimization of a working fluid for a hybrid parabolic solar dish power plant. The distribution of the thermal efficiency, Fig. 7a, provides an interesting feature: A distinct jump of the efficiency from 0.3 to 0.6 is visible at p_{cr} ~ 12.5 MPa, which can be associated with the transition from a Rankine cycle to a Brayton cycle, as seen between Figs. 7b, 8a, and 8b. Another key feature of Fig. 7a is that once the cycle transitions from a Rankine to a Brayton, the thermal efficiency of the cycle doesn't significantly change. When the cycle transition occurs, thermal efficiencies of about 0.6 are achieved.

4. Conclusions

We demonstrated a new approach to identify optimal fluids and fluid blends for power cycle working fluids, with applications in solar thermal cycles. Our direct approach, using a generalized fluid representation, allows for the optimization of a thermodynamically optimal working fluid given cycle boundary conditions, rather than relying on specific preselected mixture components.

Data availability statement

The work discussed herein in performed using open source software. Of particular importance is the CoolProp thermodynamics library. The implementation of our work into the CoolProp thermodynamic framework based on Helmholtz equations of state is discussed at length in the article.

Author contributions

Conceptualization: DB; Data curation: DB, JB; Formal Analysis: JB; Funding acquisition: DB; Investigation: JB; Methodology: DB; Project administration: DB; Resources: DB; Software: JB; Supervision: DB; Validation: JB; Visualization: JB; Writing – original draft: DB, JB; Writing – review & editing: DB.

Competing interests

The authors declare no competing interests.

References

1. Cengel et al.: Thermodynamics: An Engineering Approach. McGraw-Hill Education, 2019.
2. Rodney Allam et al.: Demonstration of the Allam cycle: An update on the development status of a high efficiency supercritical carbon dioxide power process employing full carbon capture. Energy Procedia, 114:5948–5966, 07 2017. doi: 10.1016/j.egypro.2017.03.1731.
3. Coco-Enriquez et al.: Comparison between CO_2 and other supercritical working fluids (Ethane, Xe, CH4, and N2) in line-focusing solar power plants coupled to supercritical Brayton power cycles. International Journal of Hydrogen Energy, 42(Issue 28):17611–17631, 2017, https://doi.org/10.1016/j.ijhydene.2017.02.071
4. Habibi et al.: Working fluid selection for regenerative supercritical Brayton cycle combined with bottoming ORC driven by molten salt solar power tower using energy-exergy analysis. Sustainable Energy Technologies and Assessments, 39:1–11, 2020, 10.1016/j.seta.2020.100699
5. Crespi et al.: Thermal Efficiency Gains Enabled by Using CO2 Mixtures in Supercritical Power Cycles. Energy, pages 5, 8–9, 2021, https://doi.org/10.1016/j.energy.2021.121899.
6. Valencia-Chapi et al.: Supercritical CO_2 Mixtures for Advanced Brayton Power Cycles in Line-Focusing Solar Power Plants. pages 1–18, 2019, https://doi.org/10.3390/app10010055.
7. Bell et al.: Pure and Pseudo- pure Fluid Thermophysical Property Evaluation and the Open-Source Thermophysical Property Library CoolProp. Industrial & Engineering Chemistry Research, 53(6):2498– 2508, 2014, https://doi.org/10.1021/ie4033999
8. Stanley I. Sandler. Chemical, Biochemical, and Engineering Thermodynamics. Fifth edition. John Wiley and Sons, Inc., 2017, .

9. Kenneth S. Pitzer, David Z. Lippmann, R.F. Curl Jr., Charles M. Huggins, and Donald E. Petersen. The Volumetric and Thermodynamic Properties of Fluids. II. Compressibility Factor, Vapor Pressure and Entropy of Vaporization. Journal of the American Chemical Society, pages 3433–3440, 1955, https://doi.org/10.1021/ja01618a002.
10. Giorgio Soave. Equilibrium Constants From a Modified Redlich-Kwong Equation of State. Chemical Engineering Science, Volume 27(Issue 6):1197–1203, 1972, https://doi.org/10.1016/0009-2509(72)80096-4
11. Roland Span, Eric W. Lemmon, Richard T Jacobsen, Wolfgang Wagner, and Akimichi Yokozeki. A Reference Equation of State for the Thermodynamic Properties of Nitrogen for Temperatures from 63.151 to 1000 K and Pressures to 2200 MPa. AIP: Journal of Physical and Chemical Reference Data, pages 1375, 1380, 1382, 1385–1386, 2000, https://tsapps.nist.gov/publication/get_pdf.cfm?pub_id=907386.
12. P.J. Linstrom and W.G. Mallard, Eds., NIST Chemistry WebBook, NIST Standard Reference Database Number 69, National Institute of Standards and Technology, Gaithersburg MD, 20899, https://doi.org/10.18434/T4D303, (retrieved August 7, 2022)
13. Michael J. Moran, Howard N. Shapiro, Daisie D. Boettner, and Margaret B. Bailey. Fundamentals of Engineering Thermodynamics. Ninth edition. Wiley, 2018.
14. Basem et al.: The design of a hybrid parabolic solar dish–steam power plant: An experimental study. Energy Reports, pages 1949-1965, 2022, https://doi.org/10.1016/j.egyr.2021.11.236.